International Journal of Robotics and Control Systems
Vol. 4, No. 2, 2024, pp. 606-627
ISSN 2775-2658
http://pubs2.ascee.org/index.php/ijrcs

A Novel Sea Horse Optimizer Based Load Frequency Controller for Two-Area Power System with PV and Thermal Units

Cenk Andic [a,1,*], Sercan Ozumcan [b,2], Metin Varan [c,3], Ali Ozturk [b,4]

[a] Department of Electrical Engineering, Istanbul Technical University, Istanbul 34469, Türkiye
[b] Department of Electrical and Electronics Engineering, Duzce University, Duzce 81620, Türkiye
[c] Department of Electrical Electronics Engineering, Sakarya University of Applied Sciences, Sakarya 54050, Türkiye
[1] andic18@itu.edu.tr; [2] sercan21484@ogr.duzce.edu.tr; [3] mvaran@subu.edu.tr; [4] aliozturk@duzce.edu.tr
* Corresponding Author

ARTICLE INFO

Article history
Received March 06, 2024
Revised May 01, 2024
Accepted May 07, 2024

Keywords
Load Frequency Control;
Sea Horse Optimizer;
Two-are Power System;
PV System

ABSTRACT

This study introduces the Sea Horse Optimizer (SHO), a novel optimization algorithm designed for Load Frequency Control (LFC) in two-area power systems including photovoltaic and thermal units. Inspired by the interactive behaviors of seahorses, this population-based metaheuristic algorithm leverages strategies like Brownian motion and Levy flights to efficiently search for optimal solutions, demonstrating quicker and more stable identification of global and local optima than traditional algorithms. The proposed SHO algorithm was tested in a two-region power system containing a photovoltaic system and a reheat thermal unit under three different scenarios. In the first scenario, the frequency response of the algorithm to a 0.1 p.u. load change in both regions was examined. In the second scenario, the algorithm's frequency response to sudden load changes from 0.1 p.u. to 0.4 p.u. was tested. Finally, the algorithm's frequency response was examined against different levels of solar irradiance for sensitivity analysis. This study compared the performance of the SHO-optimized controller with the optimization algorithms reported in the literature, including the Genetic Algorithm (GA), Firefly Algorithm (FA), Whale Optimization Algorithm (WOA), and Modified Whale Optimization Algorithm (MWOA). In this context, the optimization of PI controller gain parameters based on the ITAE metric resulted in SHO algorithm achieving the best performance with values of 2.5308, followed by WOA at 4.1211, FA at 7.4259, and GA at 12.1244. In tests, SHO significantly outperformed these algorithms in key performance metrics, such as Settling Time, Overshoot (M+), and Undershoot (M-). Specifically, SHO achieved 98.94% better overshoot and 85.25% reduced undershoot than GA, and concluded settling times 52.79% faster than GA in the first scenario. Similar superior outcomes were noted in subsequent tests. These results underline SHO's efficacy in enhancing system stability and control performance, marking it as a significant advancement over conventional LFC methods.

1. Introduction

The demand for electrical energy has experienced a substantial increase as a result of the expansion of industries and population growth. This demand puts pressure on power systems to provide reliable and efficient electricity supply [1]. Load Frequency Control (LFC) is an essential component in the management of power systems as it serves the crucial function of ensuring equilibrium between electricity generation and demand [2]. To ensure the effective management of system frequency within an acceptable range, the LFC mechanism is employed to regulate the power output of units in order to satisfy the power requirements [3]. LFC is a system used to prevent frequency fluctuations in electrical systems. Frequency fluctuations caused by imbalances between electricity production and consumption can lead to unwanted consequences, such as destabilizing the energy system, causing power outages, and even risking the collapse of the entire electrical grid [4]. The LFC is expected to play a crucial role in ensuring the reliability of the power grid, avoiding blackouts, and even avoiding the complete breakdown of the power grid [5].

Wind and solar power which are clean energy sources are vital for meeting global energy demands. However, their fluctuating nature poses a challenge for maintaining a stable energy system as their production relies on natural conditions that can vary throughout the day and seasons. This can cause sudden surges or drops in energy supply, which destabilizes the system [6]. To address this, LFC systems must respond quickly to changes in energy demand and supply. Traditional energy sources are more easily controlled, while renewable sources require innovative solutions like energy storage systems such as batteries [7].

Recent research has surged in exploring various controllers and optimization techniques for improving LFC. Classical Control Methods: Proportional Integral (PI) and Proportional Integral Derivative (PID) controllers have been effectively employed in LFC regulation. These controllers have been specifically examined in three-area thermal systems that integrate solar thermal power plants [8], [9]. Moreover, the effectiveness of these controllers in regulating LFC has also been explored in other complex setups [10]. Despite their simplicity, classical controllers often require considerable effort in parameter adjustment.

Physics-Inspired Algorithms: Facing the limitations of traditional controllers, many researchers have shifted towards optimization algorithms like Simulated Annealing (SA) [11], Big Bang-Big Crunch (BBBC) [12], and Gravitational Search Algorithm (GSA) [13]. Concurrently, swarm intelligence methods such as Artificial Bee Colony (ABC) [14], Ant Colony Optimization (ACO) [15], Cuckoo Search (CS) [16], and Particle Swarm Optimization (PSO) [17], [18], along with evolutionary techniques like Genetic Algorithm (GA) [19], Differential Evolution (DE) [20], Flower Pollination Algorithm (FPA) [21], Whale Optimization Algorithm (WOA) [22], Water Cycle Algorithm (WCA) [23], Grasshopper Optimization Algorithm (GOA) [24], Grey Wolf Optimizer (GWO) [25], Dragonfly Algorithm (DA) [26]-[28], Elephant Herding Optimization Algorithm (EHOA) [29], Honey Badger Algorithm (HBA) [30]-[32], Black Widow Optimization Algorithm (BWOA) [33], Firefly Algorithm (FA) [34], [35], Whale Optimization Algorithm (WOA) [36], Gorilla Troops Optimizer (GTO) [37] Quantum Gorilla Troops Optimizer [38], Brown Bear Algorithm (BBA) [39], Intuitive Algorithm (IA) [40] and RIME algorithm [41] have been applied. These meta-heuristic strategies, however, may face challenges such as getting trapped in local minima, slow convergence, and lengthy computation times for complex problems.

Artificial Intelligence Techniques: To address non-linearities in power systems, artificial intelligence approaches like Fuzzy Logic (FL) [42]-[45], Neural Networks (NN) [46], [47] and sliding mode controller [48], [49] have been adopted. These techniques face challenges such as the intensive labor required to define influential signals and the complexity of determining optimal neural network structures.

In this study, we introduce an innovative technique for tuning PI/PID load frequency controllers within a two-area power system that includes photovoltaic and reheat thermal units, using the Sea Horse Optimizer (SHO) algorithm [50]. Our primary goal is to optimize the gain parameters of these

controllers to ensure that frequency responses remain within acceptable levels despite load changes. To achieve this, we have tested the system under three different scenarios: firstly, by applying a 0.1 p.u. load change across both areas to check the controller's ability to maintain control; secondly, by implementing sudden load changes to examine if the frequency response still meets desired standards; and thirdly, through sensitivity analysis with dynamic variations in solar irradiance levels to assess if the frequency can still be adequately managed. Power systems incorporating renewable energy sources like photovoltaics are particularly challenging to control, which motivates our focus on optimizing controllers in such environments.

We chose the SHO algorithm because it is a novel approach that models the hunting and movement behaviors of seahorses, incorporating stochastic search techniques such as Brownian motion and Levy flights. This allows the algorithm to excel in searching for both local and global optima, significantly outperforming other algorithms. By leveraging the SHO algorithm, we aim to demonstrate enhanced optimization in complex, non-linear control environments. The research contributions of this study are as follows:

1. The introduction of the Sea Horse Optimizer algorithm, which represents a pioneering approach for fine-tuning the PI/PID load frequency controllers in power systems integrated with renewable energy modules, providing a significant enhancement over traditional methods.
2. The demonstration of the SHO algorithm's superior performance through rigorous testing across multiple scenarios, confirming its effectiveness in improving frequency stability, reducing settling time, and moderating overshoot and undershoot values. This confirms its potential as a valuable tool for the complex control demands of modern power systems.

By addressing the specific challenges of LFC in power systems with integrated renewable energy, this study not only fills a critical gap in current research but also sets a new standard for future innovations in power system management.

This paper is organized as follows: Section 2 presents the system modeling for a dual-area power system that includes both photovoltaic and reheat thermal units. Section 3 describes the Sea Horse Optimizer (SHO) algorithm, developed to fine-tune PI/PID load frequency controllers. Section 4 outlines the formulation of the optimization problem and discusses the application of the SHO algorithm to enhance the performance of both PI and PID controllers. Section 5 details the simulation results, illustrating the effectiveness of the proposed method under various scenarios. Finally, Section 6 concludes the paper by summarizing our findings and suggesting directions for future research.

2. System Modeling

In this research, a two-area test system depicted in Fig. 1 [35], [36] serves as the foundational model, bifurcated into two distinct zones: the first accommodates a photovoltaic (PV) installation equipped with a top-tier maximum power point tracking (MPPT) system, while the second zone houses a reheat thermal unit. The schematics and functionalities of this test environment were brought to life using the MATLAB/Simulink software suite, where individual components such as the PV array, governor mechanism, turbine assembly, reheater module, and the overarching power system were meticulously crafted through respective transfer functions, ensuring a detailed and realistic representation of each unit in the simulation landscape. The mathematical models of these components are approximated as first-order linear transfer function models. Equation (1) to (5) represent the mathematical frameworks of the system components. The utilization of the MPPT algorithm is aimed at enhancing the effectiveness of the PV system, given that the performance of a solar panel is contingent on several factors, including solar radiation intensity and ambient temperature. However, the operation of solar panels in MPPT mode indicates a constant energy production at the maximum point, technically prohibiting any frequency regulation. Consequently, the absence of frequency feedback from the PV panels in Area 1 is a reflection of this reality.

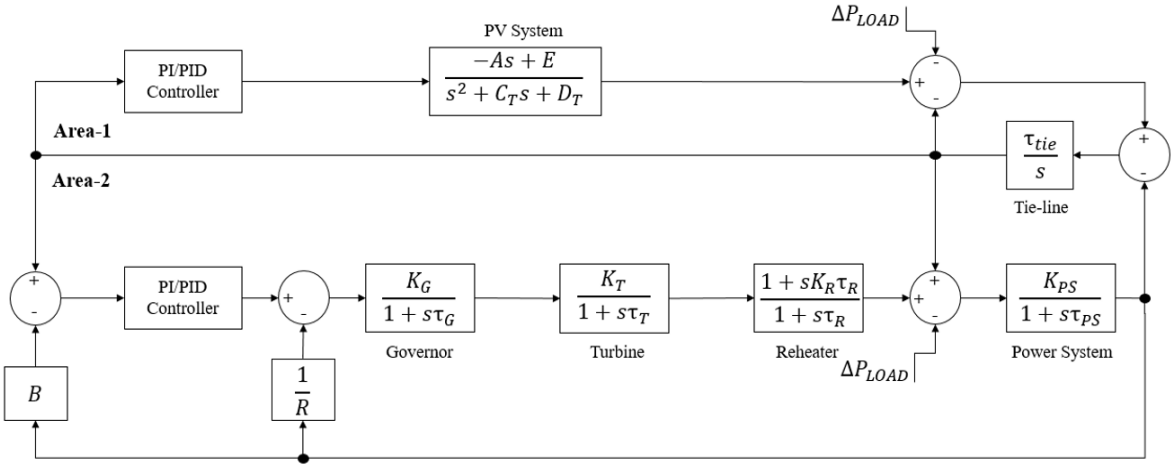

Fig. 1. The electricity distribution network that serves two distinct areas

The PV system's transfer function is delineated by Equation (1), reflecting its composite structure from diverse elements [35], [36]:

$$G_{PV} = \frac{-18s + 900}{s^2 + 100s + 50} \tag{1}$$

where the PV system's transfer function is G_{PV}. The PV system modeling encapsulates the dynamic behaviors of various photovoltaic elements which contribute to the speed and stability of energy generation. The constants within the transfer function represent the responsiveness of the panels to light and how quickly the system can adapt to changes in solar irradiance, affecting how swiftly and effectively the system responds to changes in solar input. The transfer function encapsulates the system's dynamics, allowing us to optimize its behavior. The governor's transfer function is given by following Equation (2).

$$G_{GVR} = \frac{K_G}{1 + s\tau_G} \tag{2}$$

Equation (2) represents the transfer function of the governor, $G_{GVR,}$ which regulates the power output of a generator linked to an electric grid. The governor's gain parameter, $K_{G,}$ and time constant, τ_G, play crucial roles in maintaining the stability of the power system. The governor's transfer function regulates the power output from a generator connected to the electric grid. The governor gain reflects how reactive the generator is to the load, while the time constant signifies the rate at which this reaction changes over time. These parameters dictate how swiftly and stably the system can respond to load fluctuations. The turbine's transfer function is given by following Equation (3).

$$G_{TRB} = \frac{K_T}{1 + s\tau_T} \tag{3}$$

In Equation (3), we define the transfer function of the turbine, G_{TRB}. This equation considers the turbine's gain parameter, K_T, and the time constant, τ_T, both of which impact the response time and stability of the turbine operation. The turbine's transfer function concerns the efficiency and response time of the turbine's energy generation. The turbine gain indicates how quickly energy from the generator can be converted into mechanical work, while the time constant reflects the time it takes for the turbine to respond. A fast and stable turbine is critical for the system's efficiency. The reheater's transfer function is given by following Equation (4).

$$G_{RHT} = \frac{1 + sK_R\tau_R}{1 + s\tau_R} \tag{4}$$

where the reheater's transfer function is G_{RHT}, a crucial component of the power system responsible for improving overall efficiency by recycling exhaust steam. K_R is the reheater's gain parameter, the reheater's time constant is τ_R, influence the heat transfer process and hence the overall efficiency of the power system. The reheater's transfer function is an essential component of the power system that improves overall efficiency by recycling exhaust steam for additional energy generation. The reheater gain and the time constant affect the heat transfer process and thus the overall efficiency of the energy generation process, making it a key factor in the economical and sustainable operation of the power system. The power system's transfer function is given by following Equation (5).

$$G_{PS} = \frac{K_{PS}}{1 + s\tau_{PS}} \tag{5}$$

where the power system's transfer function is G_{PS}, K_{PS} is the power system's gain parameter, τ_{PS} is the power system's time constants. The power system's transfer function represents how various inputs to the power system affect its output and stability. The power system gain and time constants are critical as they determine how quickly and effectively the system can respond to variable loads, making it a fundamental element in the control and optimization of the overall system. This equation represents how different inputs of the power system influence its output and stability, thereby playing a fundamental role in the control and optimization of the system.

3. Sea Horse Optimizer Algorithm

Introduced by Zhao in 2022, the Sea Horse Optimizer (SHO) presents a novel meta-heuristic methodology [50]. Drawing inspiration from the collaborative behavior of sea horses, the SHO algorithm functions as a population-centric meta-heuristic strategy. It is segmented into three core components: movement, hunting, and reproduction. The movement and hunting behaviors are strategically devised to foster both local and global search capacities, respectively, ensuring a harmonious blend of exploration and exploitation within the SHO framework. Reproduction serves as a complementary behavior, enriching the algorithm's holistic functionality. The SHO algorithm initializes by creating a population of candidate solutions.

$$Sea\ horses = \begin{bmatrix} x_1^1 & \cdots & x_1^{dim} \\ \vdots & \ddots & \vdots \\ x_{pop}^1 & \cdots & x_{pop}^{dim} \end{bmatrix} \tag{6}$$

where dim represents the number of dimension in the search space while pop indicates the size of the population used in the SHO algorithm. Each member of the population of seahorses corresponds to a possible solution within the problem's search space. In a minimization optimization problem, the individual with the lowest fitness value is considered as the elite individual and is denoted by X_{elite}. X_{elite} can be obtained using Equation (7).

$$X_{elite} = argmin\big(f(X_i)\big) \tag{7}$$

where $f(.)$ denotes the value of the cost function for a particular problem, which is used to evaluate the fitness of candidate solutions in the search space.

The SHO utilizes two distinctive motion behaviors inspired by the natural movement of seahorses: Brownian motion and Lévy flights. Brownian motion, characterized by random, small-step movements, enables seahorses in the SHO algorithm to thoroughly explore their immediate vicinity within the search space. This stochastic exploration is crucial for avoiding premature convergence on local optima, thus enhancing the algorithm's ability to find diverse solutions.On the other hand, Lévy flights, which involve longer, occasionally abrupt jumps, allow seahorses to leap to distant regions of the search space. This behavior is particularly effective during the early stages of the search process, where escaping local minima and exploring a broader area are vital for identifying regions with potentially superior solutions. By integrating Lévy flights, the SHO algorithm balances the exploration of new areas with the exploitation of known good regions, ensuring a comprehensive search that is

less likely to miss optimal solutions. To compute the updated position of a seahorse in iteration *t*, we can formulate these two scenarios as follows:

$$X_{new}^{1}(t+1) = \begin{cases} X_i(t) + Levy(\lambda)((X_{elite}(t) - X_i(t)) \times x \times y \times z + X_{elite}(t) & r_1 > 0 \\ X_i(t) + rand * l * \beta_t * (X_i(t) - \beta_t * X_{elite(t)} & r_1 \leq 0 \end{cases} \quad (8)$$

where $Levy$ is defined by Lévy flight distribution function with a randomly generated parameter λ from the interval [0, 2]. The spiral movement component of SHO is represented by the coordinates $x, y\ and\ z$. The constant coefficient l is used to control the step size of the Lévy flight, β_t is Brownian motion's random walk coefficient. The normal random number r_1 is used to introduce stochasticity in the Brownian motion component.

The hunting behavior in SHO is modeled to mimic the success or failure dynamics of actual seahorse hunting. Successful hunting, represented mathematically by the model, reflects a scenario where the seahorse 'captures' a near-optimal solution by effectively narrowing down the search area around the prey (optimal solution). This targeted approach helps in fine-tuning the solutions and contributes significantly to the exploitation phase, where the aim is to refine solutions close to the perceived optimum. Failure in hunting leads to further exploration, which is crucial for the algorithm to avoid local optima and to investigate more of the search space. This dynamic is fundamental to maintaining the diversity of solutions within the population, encouraging the algorithm to explore new potential areas rather than converging prematurely. The mathematical notation representing this hunting behavior can be expressed as:

$$X_{new}^{2}(t+1) = \begin{cases} \alpha * \left(X_{elite} - rand * X_{new}^{1}(t)\right) + (1-\alpha) * X_{elite}(t) & r_2 > 0.1 \\ (1-\alpha) * (X_{new}^{1}(t) - rand * X_{elite}) + \alpha * X_{new}^{1}(t) & r_2 \leq 0.1 \end{cases} \quad (9)$$

where, the new location of the sea horse after hunting at iteration *t* is denoted as $X_{new}^{1}(t)$, r_2 is the randomly generater number within [0, 1], α is a directly decreasing parameter that adjusts seahorse-based step length during the hunting process.

Reproductive behavior segregates the seahorse population into male and female groups, with the fittest individuals designated as fathers and mothers. This reproductive strategy is pivotal for genetic diversity and robustness of the algorithm. By selectively breeding the top-performing seahorses, the SHO algorithm effectively combines and propagates superior traits in the offspring, thereby continually enhancing the quality of solutions over generations. The crossover mechanism, denoted by the mixing of genetic material from selected fathers and mothers, ensures that new candidate solutions inherit the best characteristics of both parents, fostering a powerful generation of solutions capable of tackling complex optimization problems. The reproductive behavior of seahorses is split into male and female groups based on population fitness values, with male seahorses responsible for reproduction.

$$\begin{aligned} fathers &= X_{sort}^{2}(1{:}pop/2) \\ mothers &= X_{sort}^{2}(pop/2+1{:}pop) \end{aligned} \quad (10)$$

where, *fathers* and *mothers* refer to the male and female populations, respectively, while X_{sort}^{2} denotes all X_{new}^{2} arranged in ascending order of their correspoding fitness values. The algorithm selects half of the best-fit individuals from the population to create a new generation of candidate solutions. The expression of the *i*th offspring is as follows:

$$X_i^{offspring} = r_3 X_i^{father} + (1 - r_3) X_i^{mother} \quad (11)$$

where r_3 is the random number between [0, 1], X_i^{father} and X_i^{mother} individuals chosen at random from the male and female populations.

In conclusion, the integration of Brownian motion and Lévy flights for exploration and exploitation, along with strategic hunting and reproductive behaviors, empowers the SHO algorithm

to efficiently navigate and optimize within complex search landscapes. This approach not only mirrors the intriguing biological behaviors of seahorses but also translates them into a robust computational strategy that enhances the algorithm's performance in solving diverse optimization problems. Fig. 2 shows the flowchart of the proposed SHO algorithm.

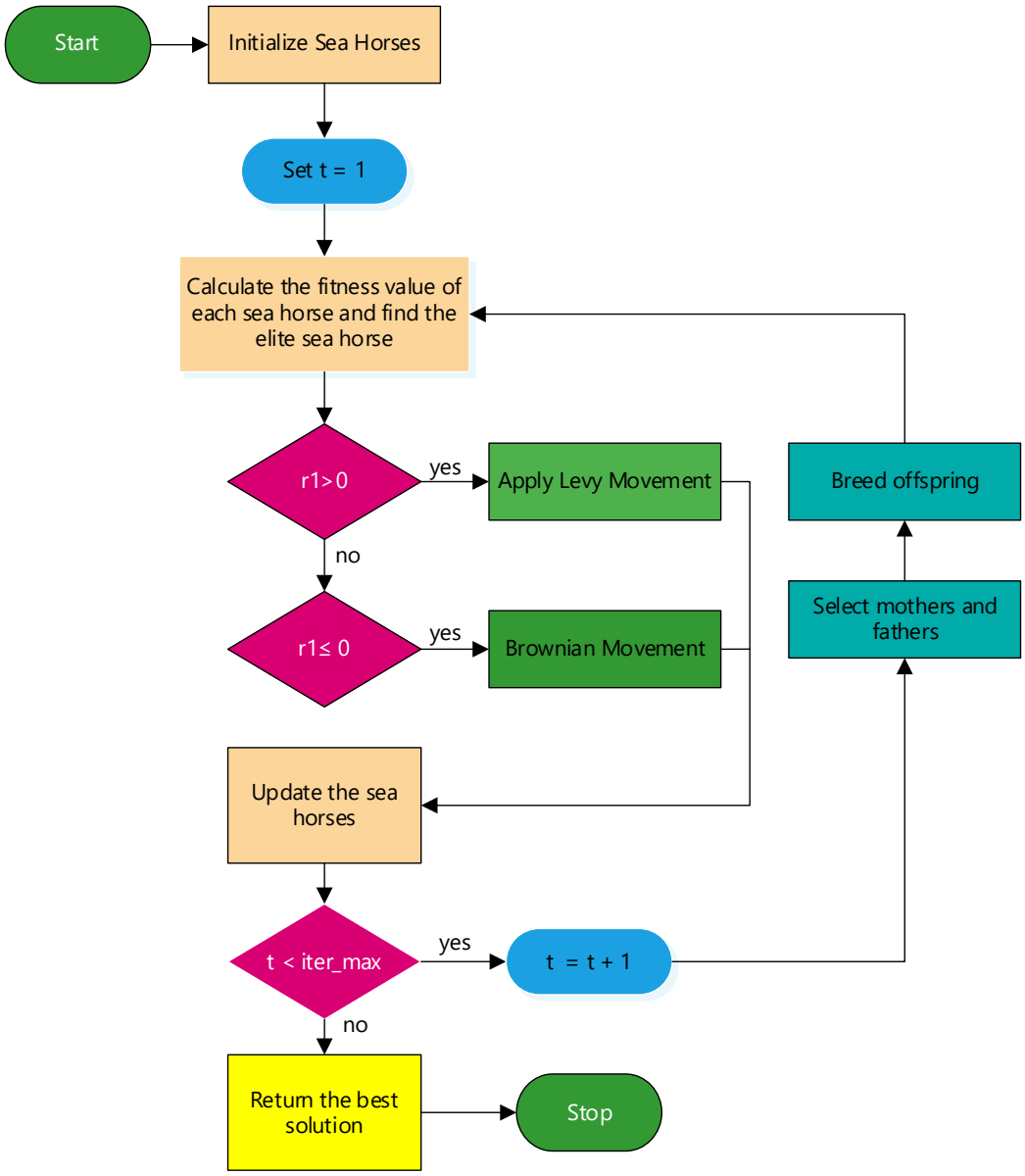

Fig. 2. A flowchart illustrating the SHO algorithm that was suggested

The SHO algorithm provides a novel approach to solving optimization problems, and its effectiveness and efficiency make it a promising technique for various applications. This study proposes the utilization of the SHO algorithm for optimizing PI/PID controllers in the LFC problem.

4. Sea Horse Optimization Based Load Frequency Control

In a power system, any discrepancy between power generation and demand can induce alterations in the system's frequency. Such frequency deviations result in the generation of a signal termed as the Area Control Error (ACE). The ACE signal serves a pivotal role, acting as a primary input for the LFC controller. This LFC controller is tasked with ensuring a balance between the total system demand and its corresponding generation. By continuously observing the ACE signal, the LFC

controller makes necessary adjustments to the power output of the generators, ensuring that the power system operates in a state of stability and reliability. From a mathematical standpoint, the ACE signals for both Area-1 and Area-2 can be articulated as:

$$ACE_1 = B_1 . \Delta F_1 + \Delta P_{tie} \quad (12)$$

$$ACE_2 = B_2 . \Delta F_2 + \Delta P_{tie} \quad (13)$$

where, B_1 and B_2 are frequency bias parameters of the both Areas 1 and 2, respectively. ΔF_1 and ΔF_2 are the frequency deviations for the both Areas 1 and 2, respectively. ΔP_{tie} is the tie-line power variation. The LFC controller can apply various strategies to manage power generation using the ACE signal. For example, the controller can increase or decrease generator outputs based on whether the ACE signal is positive or negative, which can help to mitigate power imbalances between supply and demand in the control area. Moreover, the controller is capable of regulating generator outputs based on the rate of change of the ACE signal, which is instrumental in preserving the stability of the power system.

PI or PID controllers are control strategies that are often used to reset the ACE signal. These controllers measure the ACE signal and generate the necessary control signals to keep it close to zero.

4.1. PI Controller

The PI controller is a type of feedback control that is commonly used in LFC applications. The PI controller uses two control terms to adapt the system frequency, which are the proportional term and the integral term. The proportional term acts to stabilize the frequency quickly, while the integral term acts to eliminate the steady-state error by adjusting the control signal over time. The transfer function of the PI controller is formulated as:

$$G_{PI}(s) = \left(K_p + \frac{K_i}{s}\right) \quad (14)$$

where, K_p is the proportional gain and K_i is the integral gain.

4.2. PID Controller

The PID controller is a widely adopted feedback control strategy that encompasses three key elements: proportional, integral, and derivative. It serves as an extension of the PI controller and is developed to enhance the performance of the control system, particularly with regards to stability and transient response. The transfer function of the PID controller is expressed as:

$$G_{PID}(s) = \left(K_p + \frac{K_i}{s} + K_d . s\right) \quad (15)$$

where, K_p, K_i and K_d are the proportional, integral and derivative gains, respectively. In this research, we will employ the proposed SHO algorithm to optimize the controller gains. Our primary objective function is the integral of time multiplied by the absolute error (ITAE), focusing on the frequency discrepancies in both areas as well as the variation in tie-line power. The ITAE objective function is expressed in Equation (16) and is utilized to determine the optimal controller gains, ultimately improving the power system's performance. The ITAE is a performance metric. This criterion helps optimize the controller for fast response and stable operation. ITAE calculates the integral of multiplying the controller by the error in the ACE signal at a given time and is used to evaluate the controller performance. In the context of load frequency control, selecting ITAE as the performance metric is particularly crucial because it effectively penalizes persistent frequency deviations over time. This prioritization is essential in power systems, where prolonged deviations can lead to inefficiencies and instability across the network. By optimizing controller gains to minimize ITAE, we directly target improving the system's resilience and response to frequency variations, ensuring faster adjustment to setpoints and enhanced overall stability.

$$J = \int_0^\infty t(|\Delta f_1| + |\Delta f_2| + |\Delta P_{tie}|)dt \tag{16}$$

where J is the objective function of the LFC problem. It is aimed to minimize the J. in which J represents the LFC problem's objective function. The J is expected to decrease as a result.

When optimizing PID controllers, it is necessary to constrain the gain parameters K_p, K_i and K_d within predefined lower and upper bounds. These bounds represent variable constraints that ensure the stability and performance of the controller. Equation (17) specifies the limit ranges for the PID controller.

$$\begin{aligned} K_p^{min} \le K_p \le K_p^{max} \\ K_i^{min} \le K_i \le K_i^{max} \\ K_d^{min} \le K_d \le K_d^{max} \end{aligned} \tag{17}$$

The proposed SHO algorithm aims to optimize the gain parameters of a PI/PID controller by utilizing the J objective function in Equation (16) and considering the variable constraints in Equation (17). Fig. 3 illustrates how the SHO algorithm optimizes PI/PID parameters for the LFC problem. We utilized the SHO algorithm we've put forward to address the LFC challenge, as demonstrated by the system depicted in Fig. 1. For further details regarding the test model's parameter specifications, one can refer to Table 1 [35], [36]. The suggested SHO algorithm's settings are listed in Table 2, and the LFC problem's PI/PID controller's block design is shown in Fig. 3.

Table 1. Parameters of the test system

A	PV system gain 1	18
E	PV system gain 2	900
C_T	PV system time constant 1	100
D_T	PV system time constant 2	50
K_G	Governor gain	1 p.u. MW
τ_G	Governor time constant	0.08 sec
K_T	Turbine gain	1 p.u. MW
τ_T	Turbine time constant	0.3 sec
K_r	Reheat gain	0.33 p.u. MW
τ_R	Reheat time constant	10 sec
K_{PS}	Power system gain of thermal area	120 Hz/p.u. MW
τ_{PS}	Power system time constant	20 sec
R	Regulation droop	0.4 Hz/p.u. MW
B	Frequency bias constant	0.8 p.u.
τ_{tie}	Tie-line power coefficient	0.545

Each of the parameters in Table 2 plays a certain role in the optimization process of the SHO algorithm, and understanding these roles increases the efficiency of the algorithm and its capacity to solve the LFC problem. The number of seahorses represents the diversity of solution candidates in the search space. More seahorses generally means greater diversity in the search space, which can increase the chances of finding the global optimum. It is the number of iterations the algorithm performs to reach a solution. A sufficient number of iterations allows a deeper search and potentially better solutions to be found. u, v, l: These parameters determine the step sizes that seahorses will take during Brownian motion and Levy flight. These step sizes affect the algorithm's balance of exploration and exploitation. If the value of u is chosen high, the global search ability of seahorses increases, allowing the algorithm to explore larger areas of the search space. In large and unknown search spaces, if extensive exploration is preferred before reaching the optimum, the value of u should take a large value. The v refers to the local search ability of the algorithm and enables a detailed search in small steps. If it is thought that there may be a better solution nearby, that is, if the algorithm is more in the exploitation phase, the v value can be increased. The l parameter determines the step size of Levy flights. If l takes a small value, the algorithm moves in smaller steps, which strengthens the

exploitation phase. Larger l values mean longer steps, which leads to more radical changes in the exploration phase, increasing global search capacity.

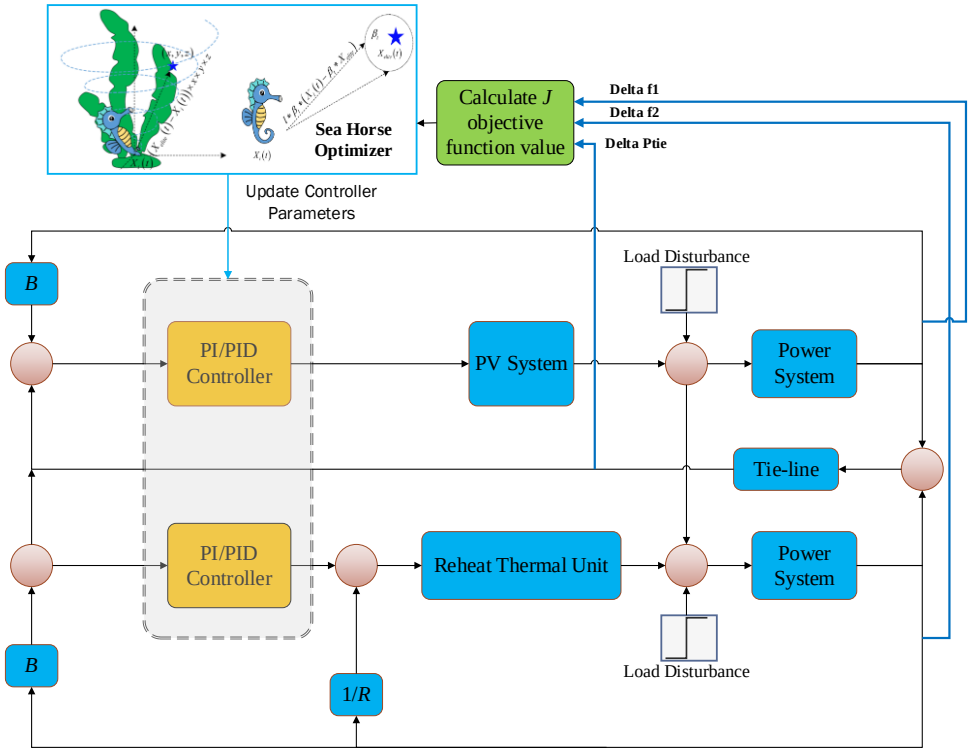

Fig. 3. The proposed SHO algorithm optimizing PI/PID parameters for LFC problem

Table 2. Comparative analysis of parameters for SHO, FA, GA, and WOA in solving LFC problem

Parameter	SHO	FA [35]	GA [35]	WOA [36]
Number of sea horse	50	50	50	50
Iteration number	100	100	100	100
u	0.05	-	-	-
v	0.05	-	-	-
l	0.05	-	-	-
Lower bound for PID $[K_p; K_i; K_d]$	[-2; -2; -2]	-	-	[-2; -2; -2]
Upper bound for PID $[K_p; K_i; K_d]$	[2; 2; 2]	-	-	[2; 2; 2]
Lower bound for PI $[K_p; K_i]$	[-2; -2]	[-2; -2]	[-2; -2]	[-2; -2]
Upper bound for PI $[K_p; K_i]$	[2; 2]	[2; 2]	[2; 2]	[2; 2]
Contrast of the attractiveness	-	1.0	-	-
Attractiveness at $r = 0$	-	0.1	-	-
Randomization parameter ($\propto$)	-	0.1	-	-
Crossover probabilities	-	-	0.75	-
Mutation probabilities	-	-	0.1	0.4
Rate of procreation	-	-	-	0.6
Rate of cannibalism	-	-	-	0.44

In the proposed SHO algorithm, the upper iteration limit is set to 100, and the sea horse population is fixed at 50 to ensure a uniform basis for comparison with other optimization algorithms, such as FA, GA, and WOA, as reported in the literature [35], [36]. The gain parameters of the controller are set within a symmetrical range of -2 to 2, aligning with comparable settings in similar studies. The effectiveness of the algorithm and its efficiency in addressing the LFC problem are highly dependent on selecting an optimal set of parameters. Therefore, for a valid comparison and to accurately gauge the SHO algorithm's performance, we have chosen parameter values that are consistent with those used in the benchmarked algorithms.

5. Simulation Results and Discussion

The SHO algorithm was implemented and run on a system equipped with an Intel i7 processor operating at 2.50 GHz and bolstered by a 16.00 GB RAM capacity, leveraging the MATLAB/Simulink software suite for execution. To affirm the robustness of the freshly proposed SHO strategy in fine-tuning the PI/PID controller gain elements, several scenarios were scrutinized. Initially, a load alteration of 10% was administered symmetrically across both zones. The second scenario examined the effect of high load demand on system stability. The third scenario investigated the influence of solar radiation variation. Finally, to evaluate the performance of the controllers, in addition to the ITAE performance index, other performance indicators such as the IAE, the ISE and the ITSE values were compared.

5.1. Scenario 1: Comparative Analysis of SHO-Optimized Controller Against Previously Documented Methods

In this setup, a dual-region system undergoes a 0.1 p.u. load disruption in both regions at the third second. The test model is adjusted using controllers optimized by several well-known optimization techniques [35], [36]. Table 3 presents the controller parameters and the fitness function outcomes derived from the SHO approach.

Table 3. PV-Thermal system's controller settings

Parameter	Methods					
	SHO-tuned PID (proposed)	**MWOA-tuned PID** [36]	**SHO-tuned PI (proposed)**	**WOA-tuned PI** [36]	**FA-tuned PI** [35]	**GA-tuned PI** [35]
K_{p1}	-0.8599	-0.1070	-0.67012	-0.4563	-0.8811	-0.5663
K_{i1}	-0.1290	-0.0906	-0.5371	-0.2254	-0.5765	-0.4024
K_{d1}	-1.9396	-0.6112	-	-	-	-
K_{p2}	-2.0000	-1.8938	-2.0000	-0.8967	-0.7626	-0.5127
K_{i2}	-2.0000	-1.8935	-0.8476	-0.9865	-0.8307	-0.7256
K_{d2}	-0.2614	-0.2505	-	-	-	-
ITAE	0.8582	1.5602	2.5308	4.1211	7.4259	12.1244
Computational Time (s)	26.7	33.8	14.1	26.9	21.7	39.8

According to Table 3, among the compared PI controllers, the SHO algorithm provides the best objective function value of 2.5308. This value represents how effectively the controller reduces the error in the ACE signal over time. Therefore, the optimal PI controller parameter values (K_{p1}= -0.67012, K_{i1}= -0.5371, K_{p2}= -2.0000 and K_{i2}= -0.8476) are obtained using the SHO algorithm. Similarly, among the compared PID controllers, the SHO algorithm provides the best objective function value of 0.8582. Therefore, the optimal PID controller parameter values (K_{p1}= -0.8599, K_{i1}= -0.1290, $K_{d1} = -1.9396$, K_{p2}= -2.0000, K_{i2}= -2.0000, $K_{d2} = -0.2614$) are obtained using the SHO algorithm. Moreover, these optimized values comply with the bound limits of the controller parameter values provided in Table 2, which range from -2 to 2.

Table 3 also includes the computational time for each of the considered PI and PID controllers. Among the PI controllers, the proposed SHO-tuned PI controller achieves the quickest computation, with a time of 14.1 seconds. This is faster than the other PI controllers, such as the WOA-tuned PI controller (26.9 seconds), FA-tuned PI controller (21.7 seconds), and GA-tuned PI controller (39.8 seconds). For the PID controllers, the proposed SHO-tuned PID also outperforms the MWOA-tuned PID by completing computations in 26.7 seconds as opposed to 33.8 seconds. Consequently, the SHO algorithm's ability to find optimal or near-optimal solutions in a shorter time underscores its robustness and practical applicability for tuning controllers in the LFC problem.

Table 4 presents the statistical analysis of fitness values for the proposed SHO-tuned PI and PID controllers. The fitness values represent the performance of the controllers, with lower values

indicating better performance. For the SHO-tuned PI controller, the worst fitness value is 4.3644, the average fitness value is 2.7406, and the best fitness value is 2.5308. The best fitness value of 2.5308 demonstrates that in 28 out of the 30 runs, the SHO-tuned PI controller outperformed the best results obtained by other methods, achieving a success rate of 93.33%. On the other hand, the SHO-tuned PID controller exhibits even better performance. It has a worst fitness value of 3.1022, an average fitness value of 1.2917, and a best fitness value of 0.8582. The best fitness value of 0.8582 reveals that, in 29 out of the 30 runs, the SHO-adjusted PID controller surpassed alternative approaches, resulting in a success rate of 96.67%. The SHO-tuned PID controller, in particular, demonstrates superior performance compared to the SHO-tuned PI controller and other methods, achieving a higher success rate.

Table 4. Statistical analysis of fitness values for proposed SHO-tuned PI and PID controllers

Methods	Fitness Value		
	Worst	Average	Best
SHO-tuned PI	4.3644	2.7406	2.5308
SHO-tuned PID	2.1022	1.1917	0.8582

In assessing the precision and efficacy of controllers for the Load Frequency Control (LFC) issue, certain performance indicators come to the fore. Notably, Settling Time stands out, serving as a gauge for the duration the controller requires to align the ACE signal near its zero mark. Settling time is a crucial stability. Overshoot (M+) and undershoot (M-) terms are also important metrics used to assess the performance of the controller. Maximum overshoot refers to the highest deviation from the reference frequency that occurs when the LFC controller stabilizes the system frequency. Undershoot occurs when the system frequency temporarily drops below the reference frequency due to the LFC controller reaching the reference frequency quickly. This may require a longer time for the system frequency to stabilize. Table 5 provides a comparison of the performance values for PI controllers.

Table 5. Characteristics of the dynamically responding system using an optimized PI controller

Parameters		GA	FA	WOA	SHO (proposed)
Δf_1	Overshoot (M^+)	0.1638	0.1577	0.07997	0.001733
	Undershoot (M^-)	-0.2966	-0.3154	-0.2015	-0.04374
	Settling Time (s)	26.73	26.44	26.30	12.62
Δf_2	Overshoot (M^+)	0.1571	0.1228	0.09816	0.1012
	Undershoot (M^-)	-0.2435	-0.2295	-0.2216	-0.1807
	Settling Time (s)	23.64	23.60	25.54	15.75
ΔP_{tie}	Overshoot (M^+)	0.05636	0.04643	0.0534	0.03823
	Undershoot (M^-)	-0.04921	-0.04778	-0.03814	-0.03215
	Settling Time (s)	27.73	26.45	21.07	18.04

Table 5 highlights the enhanced performance of the SHO-optimized PI controller when compared to other methods previously documented. It distinctly reveals reduced overshoot, undershoot, and a quicker settling time for system fluctuations. Although the frequency overshoot in the second area is marginally higher with the SHO than the WOA, the SHO-optimized controller markedly excels in diminishing undershoot and notably accelerating the response's settling time. Results show that the proposed SHO algorithm, in the first area's frequency response to overshoot (M+), is 98.94% better than GA, 98.9% better than FA, and 97.83% better than WOA. For undershoot (M-), it is 85.25% less than GA, 86.13% less than FA, and 78.29% less than WOA. It also concluded settling times 52.79% faster than GA, 52.27% faster than FA, and 52.02% faster than WOA. In the second area's frequency change, SHO showed better overshoot (M+) results by 93.59% over GA, 92.25% over FA, and 87.16% over WOA. It improved undershoot (M-) by 74.02% over GA, 80.01% over FA, and 18.43% over WOA, and it stabilized the system 33.47% faster than GA, 33.16% faster than FA, and 38.29% faster than WOA. In tie-line power changes, SHO exhibited 42.73% lower overshoot (M+) than GA, 16.99% than FA, and 28.05% than WOA. For undershoot (M-), it was 34.35% less than GA, 32.63%

less than FA, and 15.42% less than WOA, and it was faster in settling time by 33.39% compared to GA, 31.81% compared to FA, and 14.44% compared to WOA. These percentage improvements demonstrate the significant advancements and superiority of the SHO algorithm in frequency stabilization and control performance in power systems.

Fig. 4, Fig. 5, Fig. 6 showcase the simulation outcomes, illustrating the frequency shifts in both areas and the tie-line power dynamics of the power system when under the influence of an optimally tuned PI controller. The proposed SHO algorithm uses a population size of 50 while the maximum repetition limit is set to 100. However, it needs to be shown whether the SHO algorithm is stuck at a local optimum. The convergence of the proposed SHO-based PI controller to solve LFC problem is shown in Fig. 7. The fitness function value for the issue seems to settle before 100 iterations, as seen by the convergence curve in Fig. 7. Table 3 showcases the findings, underscoring that the fitness function value plateaus at 2.5308. This value notably outperforms those obtained using other optimization techniques referenced in [35] and [36].

When a PID controller is used, it is evident that the proposed SHO method yields a better objective function value of 0.8582 compared to the value of 1.5602 obtained by the MWOA [36] method. The PID controller, which has more tuning parameters, is able to respond better to frequency variations in response to load changes. Fig. 8, Fig. 9, Fig. 10 depict the frequency fluctuations in both zones and the tie-line power dynamics, following a 0.1 p.u. load disturbance in both regions, when governed by both the proposed SHO-tuned PID controller and the MWOA-tuned PID controller [36].

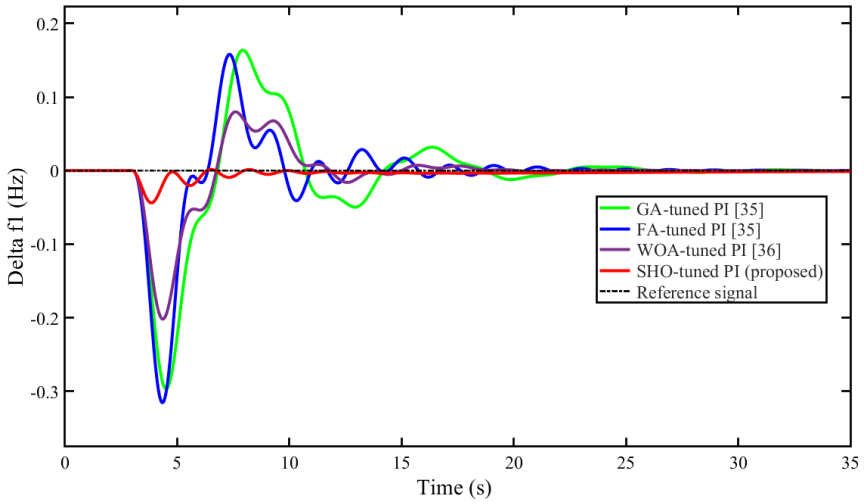

Fig. 4. Area-1 frequency reaction to load alterations in both regions utilizing PI controllers

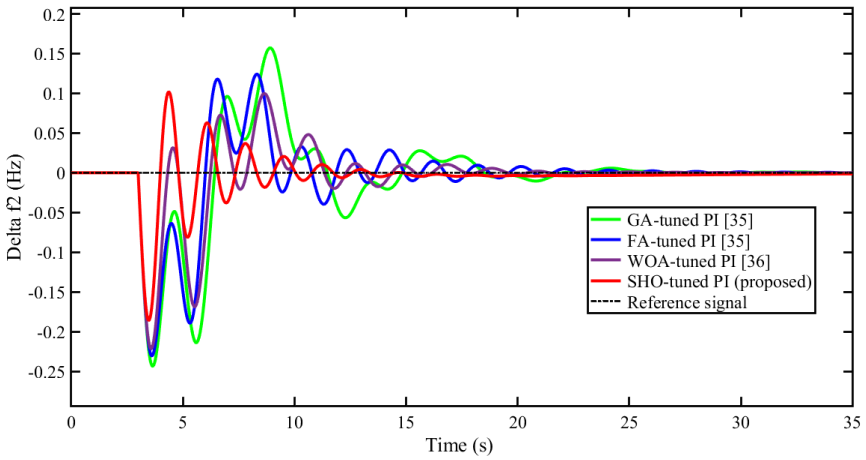

Fig. 5. Area-2 frequency reaction to load alterations in both regions utilizing PI controllers

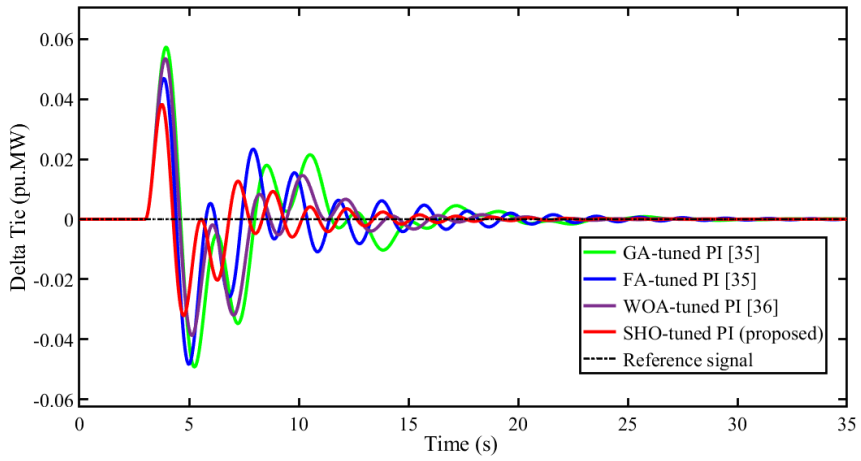

Fig. 6. Tie-line power adaptation to load variations in both zones using PI controllers

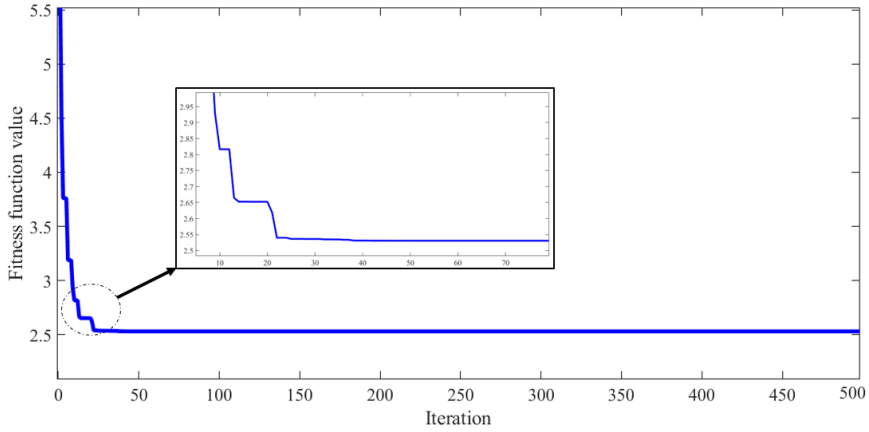

Fig. 7. Converge curve of the proposed SHO algorithm for LFC problem

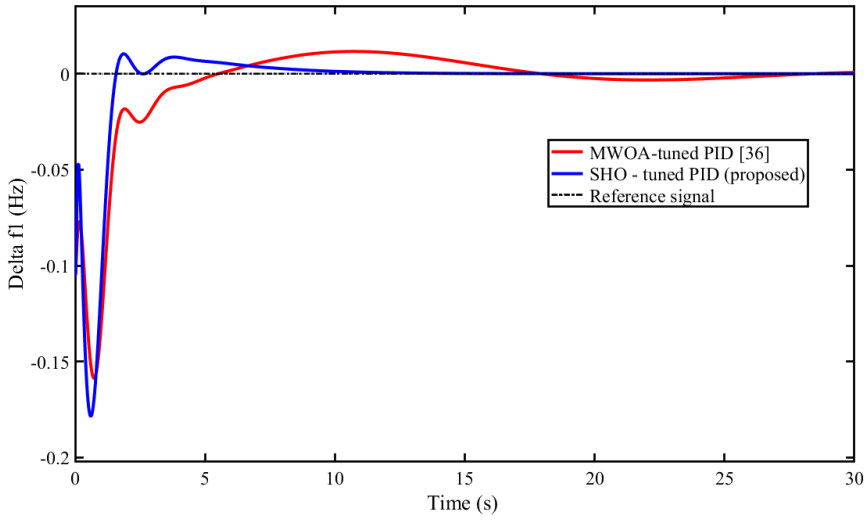

Fig. 8. Area-1 frequency reaction to load alterations in both regions utilizing PID controllers

The SHO-tuned PI method improves the fitness function by 79.11%, 65.38%, and 61.26% compared to GA, FA, and WOA methods, respectively. Additionally, the SHO-tuned PID method improves the fitness function by 45.02% compared to the MWOA method. These results demonstrate that the SHO method is a highly effective optimization algorithm for enhancing the performance of

the PI/PID controllers in LFC applications, providing more effective and reliable control of power systems.

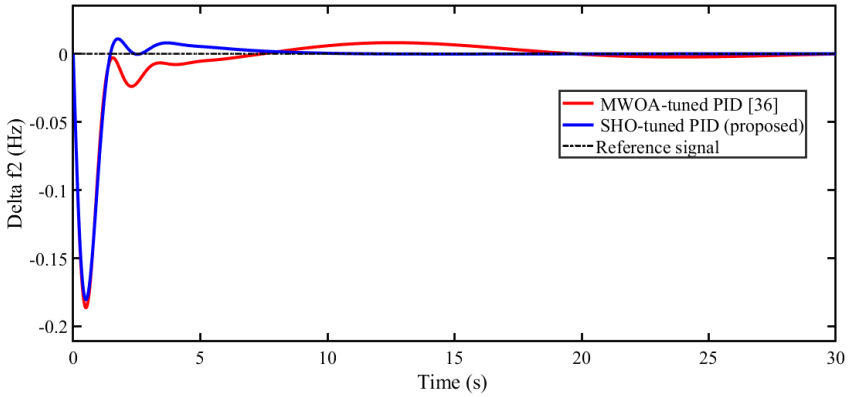

Fig. 9. Area-2 frequency reaction to load alterations in both regions utilizing PID controllers

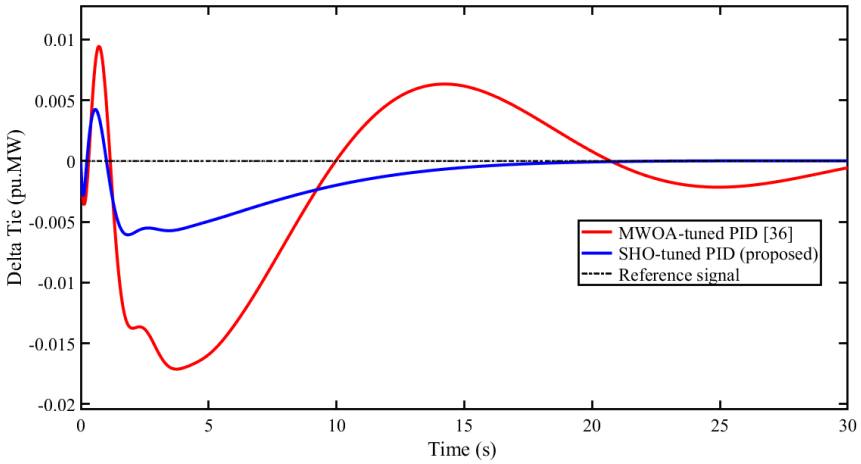

Fig. 10. Tie-line power adaptation to load variations in both zones using PID controllers

5.2. Scenario 2: Effect of High Load Demand on System Stability

In order to assess the robustness of the SHO-tuned PID controlled two-area test system, large disturbances of 0.1 p.u. to 0.4 p.u. in terms of load size were introduced suddenly during simulations. Fig. 11, Fig. 12, Fig. 13 illustrate that the system was promptly returned to a stable condition with low frequency and tie-line power variations after the suggested SHO-tuned PID controller was implemented to alleviate the effects of the disturbances. This proves that the SHO tuned PID controller is capable of keeping the system steady and reliable even when faced with extreme situations. These findings have important implications for power system design and operation with renewable energy sources, where sudden load fluctuations can pose significant challenges to grid stability.

5.3. Scenario 3: Influence of Solar Radiation Variation

In this section, we performed simulations under the assumption that solar radiation would change during the time period of t=0-100 s. To demonstrate the efficacy and robustness of the proposed SHO-based LFC method, we present and evaluate the simulation results. The simulation context considered random fluctuations in solar radiation within Area-1, depicted in Fig. 14. To gauge the effectiveness of the PID controllers fine-tuned using SHO under these conditions, we meticulously examined the system's reactions to frequency variations, namely Δf_1 and Δf_2, along with the deviation in tie-line power, denoted as ΔP_{tie}. A graphical representation of the findings is shown in Fig. 15, which provides valuable insights into the controller's ability to regulate the system under highly dynamic and uncertain conditions.

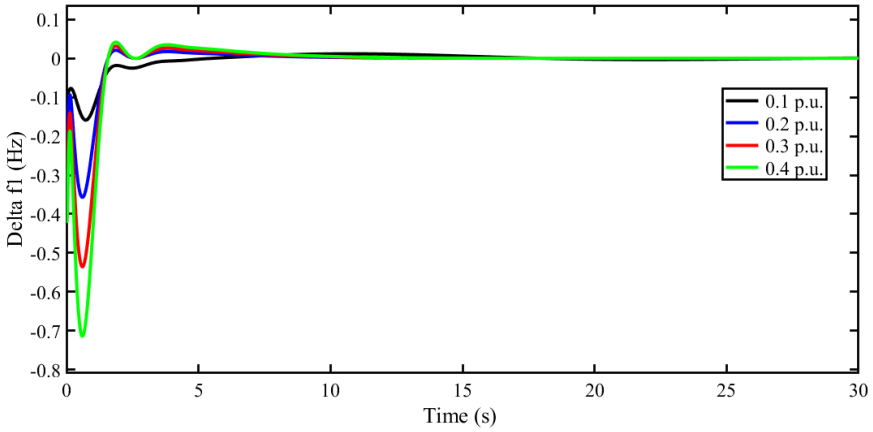

Fig. 11. Area-1 frequency reaction to major changes in load

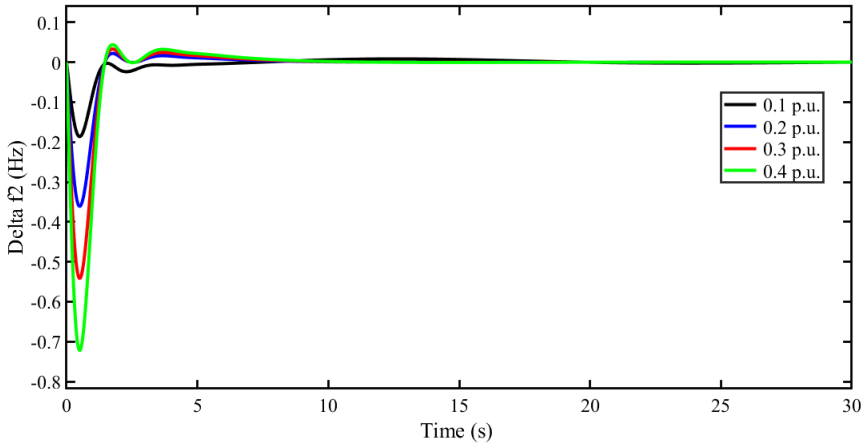

Fig. 12. Area-2 frequency reaction to major changes in load

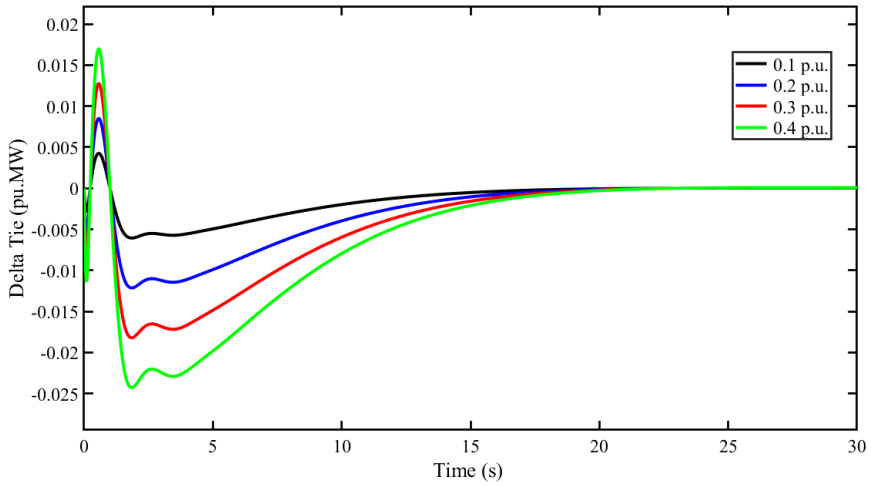

Fig. 13. Tie-line power response to major changes in load

Fig. 15 clearly illustrates that the SHO-tuned PID controllers are able to effectively regulate the system despite the fluctuations in PV power generation, maintaining the frequency and power at their desired set points. The SHO optimization approach used in tuning the PID parameters ensures that the controllers can adapt to changes in the system dynamics and provide robust control, even in the

presence of uncertainties such as random variations in PV power generation. Even with fluctuations induced by variations in solar radiation, the results highlight the efficacy and resilience of the SHO-based controller in managing power system frequency. This research underscores the potential of leveraging renewable power models for frequency control in power systems. Moreover, it emphasizes the crucial role of formulating sturdy control tactics to accommodate the unpredictability inherent in renewable power production.

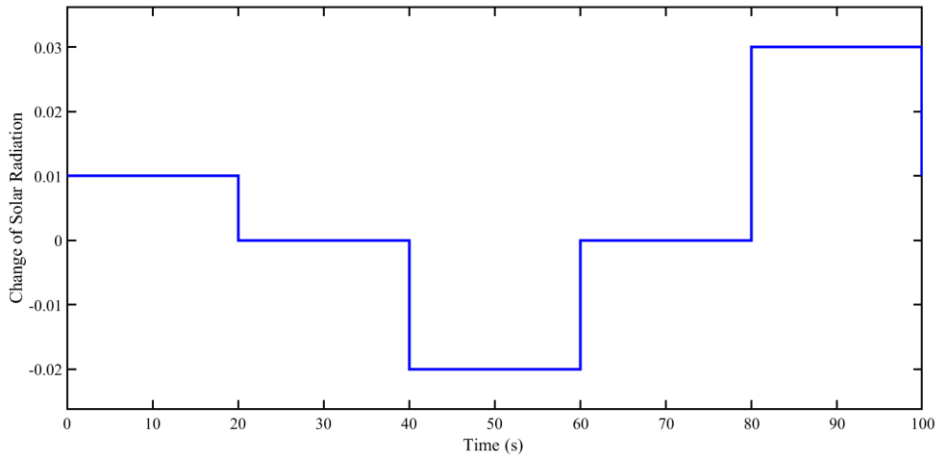

Fig. 14. Change of solar radiation

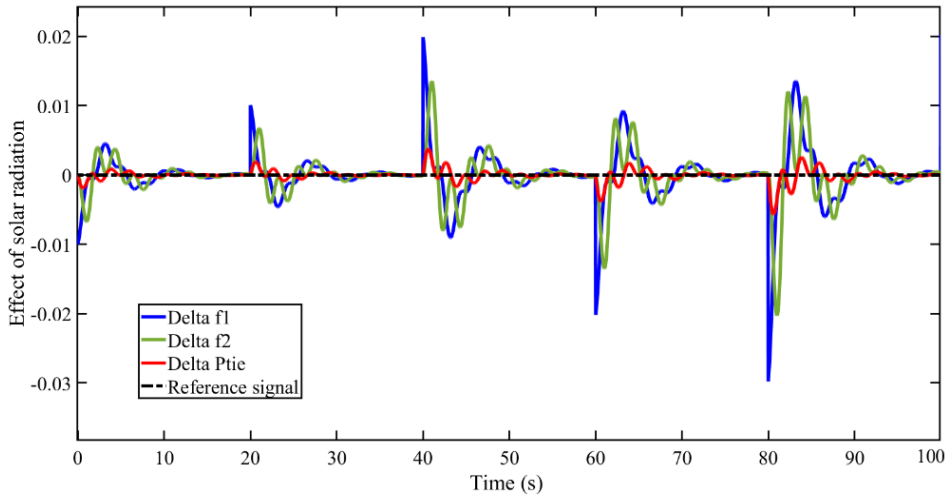

Fig. 15. Response of LFC to change in solar radiation

5.4. Robustness Measures and Performance Metrics

In our comprehensive evaluation of the developed controllers, we used several performance indices: Integral of Absolute Error (IAE), Integral of Time-weighted Absolute Error (ITAE), Integral of Squared Error (ISE), and Integral of Time-weighted Squared Error (ITSE). Each of these metrics offers insight into different aspects of controller performance, shaping our holistic understanding.

The IAE metric is often utilized when the primary concern is the overall magnitude of the error regardless of when it occurs. Minimizing IAE leads to a control action that reduces the total accumulated error, which is beneficial for systems where a fast initial response is not critical.

For ISE, the square of the error means that larger errors are penalized more heavily, which can be useful when avoiding large deviations from the setpoint is paramount. ISE tends to result in controllers that have a more aggressive response, reducing large errors quickly, but can also lead to a system that is less robust to noise.

The ITAE is particularly effective in contexts where the timing of the error is important. By penalizing errors more heavily as time progresses, ITAE tends to produce a control strategy that not only minimizes the error but also the time to settle to the desired setpoint, making it a good choice for systems where stability over time is crucial.

Lastly, ITSE integrates the time-weighted squared error, giving a measure that reflects both the magnitude and duration of errors. This can lead to a controller that provides a balance between rapid error correction and minimizing overshoots and undershoots.

These indices were computed as shown in Equations (18) through (20), with Table 6 presenting the performance indices of each tuned controller. Table 6 presents corresponding performance indices of each controller.

$$IAE = \int_0^\infty (|\Delta f_1| + |\Delta f_2| + |\Delta P_{tie}|)dt \tag{18}$$

$$ISE = \int_0^\infty ((\Delta f_1)^2 + (\Delta f_2)^2 + (\Delta P_{tie})^2)dt \tag{19}$$

$$ITSE = \int_0^\infty t((\Delta f_1)^2 + (\Delta f_2)^2 + (\Delta P_{tie})^2)dt \tag{20}$$

Table 6. Performance indices values of compared algorithms

Techniques	IAE	ITAE	ISE	ITSE
GA-tuned PI	2.3341	12.1244	0.3202	0.8618
FA-tuned PI	1.7207	7.4259	0.2907	0.4723
WOA-tuned PI	1.0566	4.1211	0.1663	0.4262
SHO-tuned PI	0.6491	2.5308	0.1021	0.26179
MWOA-tuned PID	0.5625	1.5602	0.0815	0.0601
SHO-tuned PID	0.3091	0.8582	0.0448	0.0369

Our results indicate that controllers designed using the SHO algorithm outperform those tuned with GA, FA, WOA, and MWOA across all evaluated indices. Lower values in performance indices achieved through SHO tuning point to substantial improvements in the time-domain attributes of the controllers, such as reduced overshoots and undershoots, faster settling times, and minimized sustained deviations. Consequently, SHO-tuned controllers demonstrate heightened efficacy and swiftness in regulating power system frequency in reaction to load changes, showcasing their superior capability in maintaining system stability and performance.

6. Conclusions

This study has validated the SHO algorithm's effectiveness in optimizing LFC for power systems through three distinct scenarios, demonstrating significant improvements over traditional methods like GA, FA, WOA, and MWOA. In the first scenario, with a 0.1 p.u. load change in both areas, the SHO-tuned PI controller showed a reduction in overshoot by 98.94%, undershoot by 85.25%, and settling time improvements of 52.79%, clearly outperforming the GA-tuned PI which previously held the best results. In the second scenario involving a substantial load increase, the SHO algorithm continued to maintain system stability, illustrating its robustness against high demand shocks. During the sensitivity analysis involving variations in solar irradiation, the SHO algorithm adeptly adjusted to the dynamic conditions, reducing the ITAE value by 43.72% compared to the next best method, the MWOA-tuned PID controller. The significant contribution of this study lies in demonstrating that the SHO algorithm can markedly enhance system response to load changes in power systems, significantly reducing overshoot, undershoot, and settling times in comparison to conventional methods, thereby offering a more robust and efficient approach to load frequency control. This study

establishes the SHO algorithm as a viable alternative solution method for addressing the LFC problem, demonstrating its capability to significantly enhance system response dynamics. Moreover, the SHO algorithm holds strong potential for solving other optimization problems in energy management and power systems, indicating its broad applicability and robustness in diverse operational contexts.

Author Contribution: All authors contributed equally to the main contributor to this paper. All authors read and approved the final paper.

Funding: No funding was received for this work.

Conflicts of Interest: The authors declare no conflict of interest.

References

[1] S. Yang, C. Huang, Y. Yu, D. Yue, and J. Xie, "Load frequency control of interconnected power system via multi-agent system method," *Electric Power Components and Systems*, vol. 45, no. 8, pp. 839–851, 2017, https://doi.org/10.1080/15325008.2015.1131764.

[2] W. Tan and Z. Xu, "Robust analysis and design of load frequency controller for power systems," *Electric Power Systems Research*, vol. 79, no. 5, pp. 846–853, 2009, https://doi.org/10.1016/j.epsr.2008.11.005.

[3] V. Kumar, V. Sharma, and R. Naresh, "Leader harris hawks algorithm based optimal controller for automatic generation control in PV-hydro-wind integrated power network," *Electric Power Systems Research*, vol. 214, p. 108924, 2023, https://doi.org/10.1016/j.epsr.2022.108924.

[4] H. H. Alhelou, M. E. Hamedani-Golshan, R. Zamani, E. Heydarian-Forushani, and P. Siano, "Challenges and opportunities of load frequency control in conventional, modern and future smart power systems: a comprehensive review," *Energies*, vol. 11, no. 10, p. 2497, 2018, https://doi.org/10.3390/en11102497.

[5] M. Mokhtar, M. I. Marei, M. A. Sameh, and M. A. Attia, "An adaptive load frequency control for power systems with renewable energy sources," *Energies*, vol. 15, no. 2, p. 573, 2022, https://doi.org/10.3390/en15020573.

[6] A. Singh and V. Sharma, "Salp swarm algorithm-based model predictive controller for frequency regulation of solar integrated power system," *Neural Computing and Applications*, vol. 31, pp. 8859–8870, 2019, https://doi.org/10.1007/s00521-019-04422-3.

[7] E. Celik, N. Ozturk, and E. H. Houssein, "Improved load frequency control of interconnected power systems using energy storage devices and a new cost function," *Neural Computing and Applications*, vol. 35, pp. 681–697, 2023, https://doi.org/10.1007/s00521-022-07813-1.

[8] M. H. Ibrahim, A. S. Peng, M. N. Dani, A. Khalil, K. H. Law, S. Yunus, M. I. Rahman, and T. W. Au, "A novel computation of delay margin based on grey wolf optimisation for a load frequency control of two-area-network power systems," *Energies*, vol. 16, no. 6, p. 2860, 2023, https://doi.org/10.3390/en16062860.

[9] T. Ali, S. A. Malik, A. Daraz, S. Aslam, and T. Alkhalifah, "Dandelion optimizer-based combined automatic voltage regulation and load frequency control in a multi-area, multi-source interconnected power system with nonlinearities," *Energies*, vol. 15, no. 22, p. 8499, 2022, https://doi.org/10.3390/en15228499.

[10] Z. Farooq, A. Rahman, and S. A. Lone, "Load frequency control of multi-source electrical power system integrated with solar-thermal and electric vehicle," *International Transactions on Electrical Energy Systems*, vol. 31, no. 7, p. e12918, 2021, https://doi.org/10.1002/2050-7038.12918.

[11] K. V. Chandrakala and S. Balamurugan, "Simulated annealing based optimal frequency and terminal voltage control of multi source multi area system," *International Journal of Electrical Power and Energy Systems*, vol. 78, pp. 823–829, 2016, https://doi.org/10.1016/j.ijepes.2015.12.026.

[12] N. Mbuli and W. S. Ngaha, "A survey of big bang big crunch optimization in power systems," *Renewable and Sustainable Energy Reviews*, vol. 155, p. 111848, 2022, https://doi.org/10.1016/j.rser.2021.111848.

[13] R. K. Sahu, S. Panda, and S. Padhan, "A novel hybrid gravitational search and pattern search algorithm for load frequency control of nonlinear power system," *Applied Soft Computing*, vol. 29, pp. 310–327, 2015, https://doi.org/10.1016/j.asoc.2015.01.020.

[14] H. Gozde, M. C. Taplamacioglu, and I. Kocaarslan, "Comparative performance analysis of artificial bee colony algorithm in automatic generation control for interconnected reheat thermal power system," *International Journal of Electrical Power and Energy Systems*, vol. 42, pp. 167–178, 2012, https://doi.org/10.1016/j.ijepes.2012.03.039.

[15] G. N. Nguyen, K. Jagatheesan, A. S. Ashour, B. Anand, and N. Dey, "Ant colony optimization based load frequency control of multi-area interconnected thermal power system with governor dead-band nonlinearity," *Smart Trends in Systems, Security and Sustainability*, pp. 157–167, 2018, https://doi.org/10.1007/978-981-10-6916-1_14.

[16] A. Y. Abdelaziz and E. S. Ali, "Load frequency controller design via artificial cuckoo search algorithm," *Electric Power Components and Systems*, vol. 44, no. 1, pp. 90–98, 2016, https://doi.org/10.1080/15325008.2015.1090502.

[17] S. H. Ghoshal, "Optimizations of PID gains by particle swarm optimizations in fuzzy based automatic generation control," *Electric Power Systems Research*, vol. 72, no. 3, pp. 203–212, 2004, https://doi.org/10.1016/j.epsr.2004.04.004.

[18] F. K. Abo-Elyousr and A. Y. Abdelaziz, "A novel modified robust load frequency control for mass-less inertia photovoltaics penetrations via hybrid PSO-Woa approach," *Electric Power Components and Systems*, vol. 47, no. 19-20, pp. 1744–1758, 2019, https://doi.org/10.1080/15325008.2020.1731867.

[19] H. Golpira and H. Bevrani, "A framework for economic load frequency control design using modified multi-objective genetic algorithm," *Electric Power Components and Systems*, vol. 42, no. 8, pp. 788–797, 2014, https://doi.org/10.1080/15325008.2014.893545.

[20] B. Mohanty, S. Panda, and P. K. Hota, "Controller parameters tuning of differential evolution algorithm and its application to load frequency control of multi-source power system," *International Journal of Electrical Power and Energy Systems*, vol. 54, pp. 77–85, 2014, https://doi.org/10.1016/j.ijepes.2013.06.029.

[21] K. Jagatheesan, B. Anand, S. Samanta, N. Dey, V. Santhi, A. S. Ashour, and V. E. Balas, "Application of flower pollination algorithm in load frequency control of multi-area interconnected power system with nonlinearity," *Neural Computing and Applications*, vol. 28, pp. 475–488, 2017, https://doi.org/10.1007/s00521-016-2361-1.

[22] D. Guha, P. K. Roy, and S. Banerjee, "Whale optimization algorithm applied to load frequency control of a mixed power system considering nonlinearities and PLL dynamics," *Energy Systems*, vol. 11, pp. 699–728, 2020, https://doi.org/10.1007/s12667-019-00326-2.

[23] C. N. S. Kalyan, B. S. Goud, C. R. Reddy, H. S. Ramadan, M. Bajaj, and Z. M. Ali, "Water cycle algorithm optimized type II fuzzy controller for load frequency control of a multi-area, multi-fuel system with communication time delays," *Energies*, vol. 14, no. 17, p. 5387, 2021, https://doi.org/10.3390/en14175387.

[24] T. A. Jumani, M. W. Mustafa, M. Md Rasid, N. H. Mirjat, Z. H. Leghari, and M. S. Saeed, "Optimal voltage and frequency control of an islanded microgrid using grasshopper optimization algorithm," *Energies*, vol. 11, no. 11, p. 3191, 2018, https://doi.org/10.3390/en11113191.

[25] O. Can, A. Ozturk, H. Eroglu, and H. Kotb, "A novel grey wolf optimizer based load frequency controller for renewable energy sources integrated thermal power systems," *Electric Power Components and Systems*, vol. 49, no. 15, pp. 1248–1259, 2022, https://doi.org/10.1080/15325008.2022.2050450.

[26] A. M. Abdel-Hamed, A. Y. Abdelaziz, and A. El-Shahat, "Design of a 2DOF-PID control scheme for frequency/power regulation in a two-area power system using dragonfly algorithm with integral-based weighted goal objective," *Energies*, vol. 16, no. 1, p. 486, 2023, https://doi.org/10.3390/en16010486.

[27] E. Çelik, "Design of new fractional order PI–fractional order PD cascade controller through dragonfly search algorithm for advanced load frequency control of power systems," *Soft Computing*, vol. 25, pp. 1193–1217, 2021, https://doi.org/10.1007/s00500-020-05215-w.

[28] E. Çelik, N. Öztürk, Y. Arya, and C. Ocak, "(1 + PD)-PID cascade controller design for performance betterment of load frequency control in diverse electric power systems," *Neural Computing and Applications*, vol. 33, pp. 15433–15456, 2021, https://doi.org/10.1007/s00521-021-06168-3.

[29] S. Dewangan, T. Prakash, and V. Pratap Singh, "Design and performance analysis of elephant herding optimization based controller for load frequency control in thermal interconnected power system," *Optimal Control Applications Methods*, vol. 42, no. 1, pp. 144–159, 2021, https://doi.org/10.1002/oca.2666.

[30] C. Andic, S. Ozumcan, A. Ozturk and B. Turkay, "Honey Badger Algorithm Based Tuning of PID Conroller for Load Frequency Control in Two-Area Power System Including Electric Vehicle Battery," *2022 4th Global Power, Energy and Communication Conference (GPECOM)*, pp. 307-310, 2022, https://doi.org/10.1109/GPECOM55404.2022.9815701.

[31] S. Ozumcan, A. Ozturk, M. Varan, C. Andic, "A novel honey badger algorithm based load frequency controller design of a two-area system with renewable energy sources," *Energy Reports*, vol. 9, pp. 272–279, 2023, https://doi.org/10.1016/j.egyr.2023.10.002.

[32] O. Can and M. Ş. Ayas, "Fractional high-order differential feedback controller based on meta-heuristic algorithms for automatic voltage regulator," *Electrical Power Components and Systems*, pp. 1-14, 2024, https://doi.org/10.1080/15325008.2024.2344200.

[33] P. Dahiya and A. K. Saha, "Frequency Regulation of Interconnected Power System Using Black Widow Optimization," *IEEE Access*, vol. 10, pp. 25219-25236, 2022, https://doi.org/10.1109/ACCESS.2022.3155201.

[34] S. Padhan, R. K. Sahu, and S. Panda, "Application of firefly algorithm for load frequency control of multi-area interconnected power system," *Electric Power Components and Systems*, vol. 42, no. 13, pp. 1419–1430, 2014, https://doi.org/10.1080/15325008.2014.933372.

[35] S. M. Abd-elazim and E. S. Ali, "Load frequency controller design of a two-area system composing of PV grid and thermal generator via firefly algorithm," *Neural Computing and Applications*, vol. 30, pp. 607–616, 2018, https://doi.org/10.1007/s00521-016-2668-y.

[36] R. K. Khadanga, A. Kumar, and S. Panda, "A novel modified whale optimization algorithm for load frequency controller design of a two-area power system composing of PV grid and thermal generator," *Neural Computing and Applications*, vol. 32, pp. 8205–8216, 2020, https://doi.org/10.1007/s00521-019-04321-7.

[37] O. Can and M. Ş. Ayas, "Gorilla troops optimization-based load frequency control in PV-thermal power system," *Neural Computing and Applications*, vol. 36, pp. 4179-4193, 2024, https://doi.org/10.1007/s00521-023-09273-7.

[38] M. A. El-Dabah, M. H. Hassan, S. Kamel and H. M. Zawbaa, "Robust Parameters Tuning of Different Power System Stabilizers Using a Quantum Artificial Gorilla Troops Optimizer," *IEEE Access*, vol. 10, pp. 82560-82579, 2022, https://doi.org/10.1109/ACCESS.2022.3195892.

[39] S. K. Ojha and C. O. Maddela, "Load frequency control of a two-area power system with renewable energy sources using brown bear optimization technique," *Electrical Engineering*, pp. 1-25, 2023, https://doi.org/10.1007/s00202-023-02143-4.

[40] K. Soyacikgoz and N. Inanc, "Designing an intuitive algorithm based load frequency controller for electrical power systems," *Electric Power Components and Systems*, pp. 1-11, 2023, https://doi.org/10.1080/15325008.2023.2267550.

[41] S. Ekinci, Ö. Can, M. Ş. Ayas, D. Izci, M. Salman and M. Rashdan, "Automatic Generation Control of a Hybrid PV-Reheat Thermal Power System Using RIME Algorithm," *IEEE Access*, vol. 12, pp. 26919-26930, 2024, https://doi.org/10.1109/ACCESS.2024.3367011.

[42] D. K. Chaturvedi, R. Umrao, and O. P. Malik, "Adaptive polar fuzzy logic based load frequency controller," *International Journal of Electrical Power and Energy Systems*, vol. 66, pp. 154–159, 2015, https://doi.org/10.1016/j.ijepes.2014.10.024.

[43] E. Cam, "Application of fuzzy logic for load frequency control of hydroelectrical power plants," *Energy Conversion and Management*, vol. 48, no. 4, pp. 1281–1288, 2007, https://doi.org/10.1016/j.enconman.2006.09.026.

[44] A. H. Yakout, H. Kotb, H. M. Hasanien and K. M. Aboras, "Optimal Fuzzy PIDF Load Frequency Controller for Hybrid Microgrid System Using Marine Predator Algorithm," *IEEE Access*, vol. 9, pp. 54220-54232, 2021, https://doi.org/10.1109/ACCESS.2021.3070076.

[45] H. A. Yousef, K. AL-Kharusi, M. H. Albadi and N. Hosseinzadeh, "Load Frequency Control of a Multi-Area Power System: An Adaptive Fuzzy Logic Approach," *IEEE Transactions on Power Systems*, vol. 29, no. 4, pp. 1822-1830, 2014, https://doi.org/10.1109/TPWRS.2013.2297432.

[46] D. K. Chaturvedi, P. S. Satsangi, and P. K. Kalra, "Load frequency control: a generalized neural network approach," *International Journal of Electrical Power and Energy Systems*, vol. 21, no. 6, pp. 405–415, 1999, https://doi.org/10.1016/S0142-0615(99)00010-1.

[47] S. D. Al-Majidi, M. Kh. AL-Nussairi, A. J. Mohammed, A. M. Dakhil, M. F. Abbod, and H. S. Al-Raweshidy, "Design of a load frequency controller based on an optimal neural network," *Energies*, vol. 15, no. 17, p. 6223, 2022, https://doi.org/10.3390/en15176223.

[48] B. Begum *et al*., "Application of an intelligent fuzzy logic based sliding mode controller for frequency stability analysis in a deregulated power system using OPAL-RT platform," *Energy Reports*, vol. 11, pp. 510-534, 2024, https://doi.org/10.1016/j.egyr.2023.12.023.

[49] A.-T. Tran, M. P. Duong, N. T. Pham, J. W. Shim, "Enhanced sliding mode controller design via meta-heuristic algorithm for robust and stable load frequency control in multi-area power systems," *IET Generation, Transmission & Distribution*, vol. 18, no. 3, pp. 460-478, 2024, https://doi.org/10.1049/gtd2.13077.

[50] S. Zhao, T. Zhang, S. Ma, and M. Wang, "Sea-horse optimizer: a novel nature-inspired meta-heuristic for global optimization problems," *Applied Intelligence*, vol. 53, pp. 11833–11860, 2022, https://doi.org/10.1007/s10489-022-03994-3.